Proceedings of the ASME 2024 International Technical Conference and Exhibition on Packaging and Integration of Electronic and Photonic Microsystems
InterPACK2024
October 8-10, 2024, San Jose, California

InterPACK2024-141775

ADDITIVELY MANUFACTURED COLD PLATE INTEGRATED WITH EVAPORATOR WICKS AND PHASE SEPARATORS FOR THERMAL MANAGEMENT OF MULTIPLE HIGH-HEAT-FLUX HEAT SOURCES

Mohammad Reza Shaeri, Maksym Demydovych, Chien-Hua Chen
Advanced Cooling Technologies, Inc., Lancaster, PA 17601, USA

ABSTRACT

In this study, a Hybrid Two-Phase Cooling System (HTPCS) was developed, combining the advantages of capillary-driven evaporation from wick structures with pumped two-phase cooling. The cold plate, the core element of the HTPCS, was made of AlSi10Mg and incorporated seven heaters distributed in a non-patterned configuration across its surface. Each heater was assigned a wick structure as an evaporator. The key contribution of this study lies in (i) fabricating the entire cold plate through one single additive manufacturing (AM) process, and (ii) preventing the flooding of individual evaporators using an internal phase separator. The first merit results in a substantial reduction in fabrication complexity compared to traditional manufacturing processes, representing a crucial milestone in the path toward commercializing the developed HTPCS in this study. The second merit results in a further reduction in the thermal resistance of the cold plate. The HTPCS exhibited significant thermal performance, operating at heat fluxes exceeding 505 W/cm^2 and achieving low and uniform thermal resistances of ~0.16 K-cm^2/W. Furthermore, the HTPCS operated within a low pumping power range, below 0.14 W. This study introduces a promising cooling technology for the thermal management of the next generation of miniaturized electronic devices, especially those integrating multiple high-heat-flux heat sources.

Keywords: Hybrid two-phase cooling; Pumped two-phase cooling; Capillary-driven cooling; Phase separator; Additive manufacturing.

NOMENCLATURE

H_C, W_C, L_C	Height, width, and length of the cold plate (m)
H 1–H 7	Heater 1 to heater 7
L_e	Length of evaporator wick (m)
t_w, W_w, L_w	Thickness, width, and total length of wick (m)
D_{in}, D_v, D_e	Diameter of the inlet, vapor outlet, and excess flow outlet manifolds (m)
H_p	Height of the pedestal (m)
W_p, L_p	Pedestal's width and length attached to the cold plate (m)
q_i	Heat flux applied to the *i*-th pedestal (W/cm^2)
R_i	Specific thermal resistance of *i*-th heater (K-cm^2/W)
t_p	Thickness of phase separator (m)
T_{in}, T_{out}	Inlet and outlet temperature (ºC)
ρ	Liquid density (kg/m^3)
$\dot{V}$	Volume flow rate (m^3/s)
c_p	Specific heat (J/kg K)
ϕ	Heat transfer ratio
I_i	Current applied to the *i*-th heater (A)
V_i	Voltage applied to the *i*-th heater (V)
$T_{s,i}$	Source temperature of the *i*-th heater (ºC)
$T_{o,v}$	Outlet temperature at the vapor line (ºC)

1. INTRODUCTION

The rapid increase in the power of electronic devices, coupled with a reduction in their size, has posed significant challenges for the thermal management of high-heat-flux electronic devices [1–4]. Removing significant amounts of concentrated heat from small areas while maintaining the temperature of electronic devices below their specified limits exceeds the capability of air-cooled systems, attributed to the poor thermal properties of air, as well as single-phase liquid cooling systems, which require large pumping power [1,5]. Compared to single-phase cooling systems, two-phase cooling technologies can absorb substantially greater amounts of heat while keeping surface temperatures relatively low due to using both the sensible and latent heat of the coolant [6]. However, the rapid miniaturization of electronics presents challenges for standalone two-phase cooling technologies. Capillary-driven evaporation from wicks has been identified as one of the most efficient passive two-phase cooling technologies for removing substantial amounts of heat without the need for external power [7]. Wick structures enable a greater coverage of the liquid meniscus by a thin film, resulting in increased rates of heat transfer through evaporation. Moreover, wicks play a crucial role in enhancing the capillary action, thereby effectively delaying the dryout by promoting the spreading of the working fluid [8]. However, the upper limit operation of a cooling system relying on capillary-driven evaporation is constrained by the capillary pressure of the wick structure [9]. Although this limitation can be resolved by pumped two-phase cooling systems like

micro/minichannel heat sinks, these cooling systems are susceptible to severe constraints, such as flow boiling instabilities that result in premature critical heat flux (CHF) [10,11].

To overcome the limitations of individual two-phase cooling technologies in the thermal management of high-heat-flux electronics, Hybrid Two-Phase Cooling Systems (HTPCSs) have been developed and demonstrated as advanced cooling technologies [12–14]. These systems combine capillary-driven evaporation from wicks with pumped two-phase cooling. Since the total pressure head of a HTPCS is set by the sum of the maximum capillary pressure head developed in the evaporator wick and the pressure head of the mechanical pump, a HTPCS allows for increasing the pressure head of the system indefinitely by selecting a proper mechanical pump [15]. Particularly, in the study by Shaeri et al. [12], the innovative aspect of the HTPCS lay in incorporating an internal phase separator made of rubber to prevent liquid from flowing over the evaporators and, consequently, to avoid flooding of evaporator wicks. However, the practical application of this HTPCS necessitates further exploration, particularly on the cold plate side. The current versions of the cold plate in the developed HTPCS in [12] undergo multiple labor-intensive steps, including CNC machining of various components of the cold plate, intricate cutting and extrusion processes for preparing a rubber phase separator, insertion of the phase separator inside the cold plate with secure placement, and bonding processes for cold plate assembly. These processes are time-consuming, costly, and demand specific fabrication tools. Furthermore, conventional fabrication methods face significant challenges, often resulting in failure, when attempting to manufacture cold plates with intricate geometries and customized internal features. All these limitations pose obstacles to the commercialization of HTPCS. The objective of this study is to overcome these challenges by fabricating the HTPCS's cold plate through one single additive manufacturing (AM) process. The AM surpasses traditional manufacturing methods in terms of production flexibility, design complexity, internal structure design, and, most notably, the throughput time for small-batch customized production [16].

2. EXPERIMENT

The schematic of the HTPCS developed in this study is illustrated in FIGURE 1. This cooling system integrates a mechanically pumped two-phase loop with capillary-driven evaporation from wicks. The HTPCS comprised a cold plate, a reservoir, multiple heat exchangers functioning as condensers, and a positive displacement pump. The loop components were interconnected through stainless steel tubes, and the working fluid chosen was refrigerant R245fa. To measure fluid temperatures and pressures at various points in the loop, such as the inlet and outlet manifolds, Resistance Temperature Detectors (RTDs) and pressure transducers were employed. Flow rate adjustments were made using a control valve and bypass situated after the pump, and measurements were taken with a turbine flowmeter located upstream of the cold plate's inlet manifold.

The CAD model of the cold plate is shown in FIGURE 2. The cold plate comprised an inlet, an excess flow outlet, and a vapor outlet. The inlet was subdivided into seven identical inlet manifolds, each forming the inlet manifold for an individual channel. Similarly, the excess flow outlets and vapor outlets of the seven channels were merged to establish the primary excess flow outlet manifold and primary vapor outlet manifold, respectively.

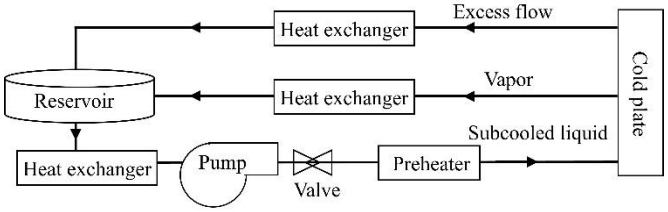

FIGURE 1: SCHEMATIC OF THE HTPCS

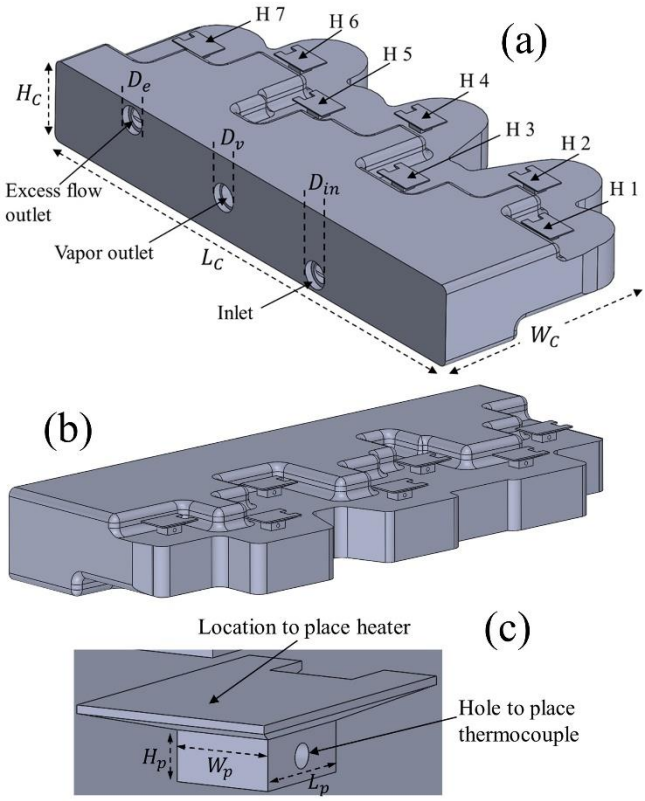

FIGURE 2: (a) THREE-DIMENSIONAL VIEW OF THE COLD PLATE, (b) THE COLD PLATE FROM A VIEWPOINT OPPOSITE TO THE INLET AND OUTLET MANIFOLDS, (c) PEDESTAL

The cold plate featured seven pedestals situated on one side and randomly distributed across its surface. These pedestals were locations to hold the heaters. In FIGURE 2(a) H 1 to H 7 represent heaters numbered 1 to 7, respectively. Initially, the HTPCS was designed for heat removal from transistors with the footprint areas of $L_p \times W_p$, as shown in FIGURE 2(c). However, due to the unavailability of off-the-shelf heaters matching the same footprint size, converging pedestals were fabricated to

accommodate heaters on the larger footprint area. A high frequency/RF resistor with a power rating of up to 200 W was affixed to the larger footprint area of each pedestal using a thermal interface material. To ensure continuous contact between each heater and its corresponding pedestal, a heater holder unit was created. This unit incorporated seven screws that pressed the heaters into the pedestals, ensuring sustained contact throughout the entire experiment. Electrical heat was applied to each pedestal through a resistive heater, with the current and voltage regulated by a variable transformer. Within each pedestal, a hole was created and extended to the midpoint to measure the source temperature using a T-type thermocouple. Thermal grease filled the space between the thermocouple and the hole. The interior of the cold plate and the CAD model of the wick structure are shown in FIGURE 3 and FIGURE 4, respectively.

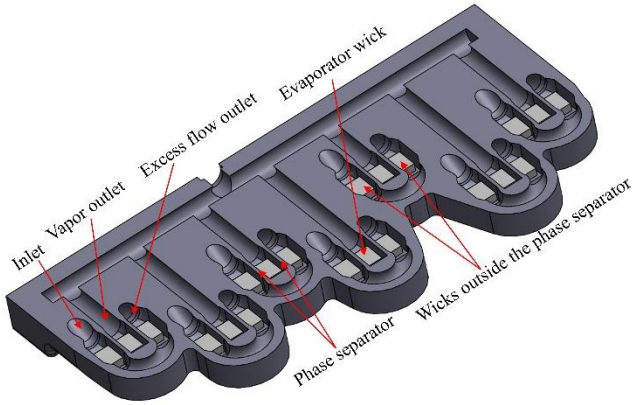

FIGURE 3: INSIDE THE COLD PLATE SHOWING THE EVAPORATOR WICK AND PHASE SEPARATOR FOR INDIVIDUAL HEATER

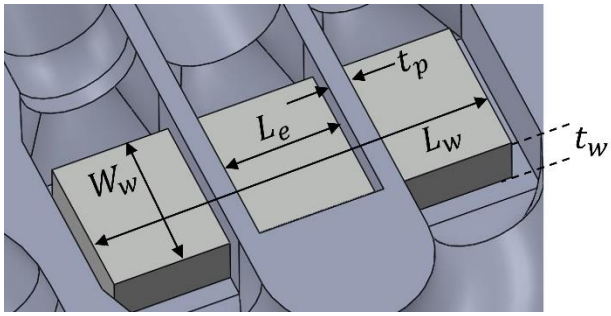

FIGURE 4: CAD MODEL OF THE WICK STRUCTURE

The heat removal from each individual heater occurred through a flow passage positioned beneath each heater. This flow passage comprised an inlet, two outlet manifolds, an evaporator wick, and a phase separator. The mechanical pump continuously supplied the cold plate with liquid. A portion of this liquid was drawn into the evaporator wicks from wick structures located outside the phase separator. Within the vapor section, the liquid underwent evaporation from the wicks. The remaining flow outside the vapor section, termed excess flow, might be two-phase due to boiling/evaporation of liquid outside the vapor section. The excess flow was redirected within the cold plate and then exited from the cold plate on the same side as the inlet manifold. The vapor pressure inside the vapor section facilitated the release of vapor generated by evaporation to the exterior of the cold plate. Consequently, throughout the entire cooling process, the evaporator wicks within the vapor section remained completely isolated from the liquid outside the vapor section. This separation is crucial to prevent the flooding of the evaporators. While the inlet and outlet manifolds were situated on the same side, there are no restrictions on their positioning, as long as vapor and liquid inside the cold plate are separated by a separator and exit the cold plate through distinct manifolds. The vapor and excess flow leaving the cold plate were directly returned to their respective condensers (i.e., heat exchangers). The outflows from both condensers were combined in the liquid reservoir. To prevent cavitation in the pump, a condenser was implemented before the pump to ensure that the inlet flow to the pump remained single-phase liquid. Then, the subcooled liquid was pumped into the cold plate, completing the loop. The heat rejected from all condensers was exchanged with lower-temperature water, supplied by a chiller.

The additively manufactured cold plate is illustrated in FIGURE 5. The cold plate, made of AlSi10Mg, was fabricated through one single AM process utilizing Direct Metal Laser Sintering (DMLS) technology. The wicks were fabricated using laser powder bed fusion of AlSi10Mg powder. A representative SEM micrograph of a sample of wick is shown in FIGURE 6.

FIGURE 5: ADDITIVELY MANUFACTURED COLD PLATE

The fabrication of the cold plates involved controlling the build parameters, including laser power, exposure time, hatch distance, point distance, and layer thickness. To ensure the removal of residual powder, the cold plate underwent a

continuous methanol flush in an in-house methanol bath. The hermeticity of the cold plate was demonstrated using a helium mass spectrometer, revealing a measured leak rate lower than 9×10^{-10} std. cc/s. The geometrical information for both the cold plate and the evaporator wicks is listed in TABLE 1.

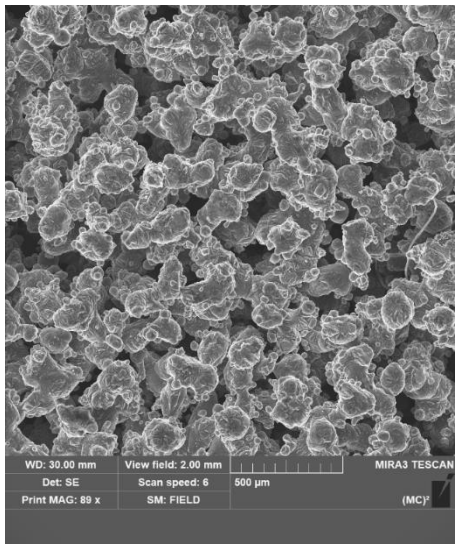

FIGURE 6: SEM IMAGE OF EVAPORATOR WICKS

TABLE 1: GEOMETRICAL INFORMATION OF THE COLD PLATE AND EVAPORATOR WICKS.

L_C, W_C, H_C	127 mm, 54.9 mm, 18.8 mm
L_e, L_w, W_w, t_w	4.8 mm, 15.24 mm, 5.5 mm, 2.0 mm
t_p	0.8 mm
L_p, W_p, H_p	3.8 mm, 3.0 mm, 1.5 mm
D_{in}, D_v, D_e	6.4 mm, 6.4 mm, 6.4 mm

Prior to conducting the experiment, the entire loop was thoroughly checked to detect any leaks before charging the loop with the refrigerant R245fa. The liquid was circulated throughout the loop, and then the pump speed and the control valve were adjusted to provide the cold plate with the desired flow rate of 1.0 LPM (liters per minute). By regulating the chiller temperature, the inlet temperature to the cold plate was consistently maintained within a narrow range, with an average temperature of 18.4°C. Under steady-state conditions, signals from the RTDs, pressure transducers, flowmeters, T-type thermocouples, and heaters were collected by a data acquisition system. The steady-state condition was identified when fluctuations in temperatures, as observed by RTDs and T-type thermocouples within the pedestals, remained minimal over an extended period of system operation.

The heat loss was determined by conducting a series of single-phase cooling tests and calculating the heat transfer ratio, which represents the ratio of heat absorbed by the working fluid to the electrical heat input, as follows:

$$\phi = \frac{\rho \dot{V} c_p (T_{out} - T_{in})}{\sum_{i=1}^{8} V_i \times I_i} \quad (1)$$

then, the heat flux to the *i*-th pedestal was calculated as follows:

$$q_i = \phi \frac{V_i \times I_i}{L_p \times W_p} \quad (2)$$

The thermal performance of the cold plate was assessed by the specific thermal resistance of the *i*-th heater, as follows:

$$R_i = \frac{T_{s,i} - \left(\frac{T_{in} + T_{o,v}}{2}\right)}{q_i} \quad (3)$$

where $T_{s,i}$ is the source temperature of the *i*-th heater, measured using the thermocouple located within the *i*-th pedestal's hole, T_{in} is the inlet temperature at the main inlet manifold, and $T_{o,v}$ is the temperature at the main vapor outlet manifold.

3. RESULTS AND DISCUSSION

The cold plate was tested horizontally with all heaters positioned on its upper surface, as shown in FIGURE 2(a). The thermal resistances of the cold plate at different heat fluxes are shown in FIGURE 7.

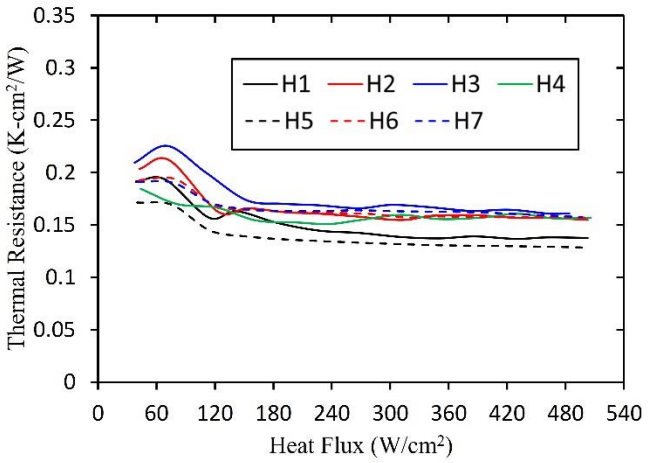

FIGURE 7: SPECIFIC THERMAL RESISTANCES AT DIFFERENT HEAT FLUXES

An increase in the heat load leads to an enhancement of evaporation, resulting in a decrease in thermal resistance. This trend continues until a global minimum thermal resistance is reached, indicating partial dryout. Partial dryout signifies an imbalance between the rate of liquid depletion from the evaporator and the rewetting capability of the evaporator. Beyond partial dryout, additional increments in the heat load result in an elevation of thermal resistance, raising the risk of CHF. In this work, CHF was recognized by a sharp increase in

the temperature of any of the seven heaters. Based on FIGURE 7, the heaters of the HTPCS functioned at heat fluxes exceeding 505 W/cm^2 without exhibiting any indications of partial dryout. The measured thermal resistances in this heat flux range were ~0.16 K-cm^2/W. The fact that partial dryout did not occur in the HTPCS suggested the capability of cold plate to operate at elevated heat fluxes. However, the experiment did not advance beyond the maximum heat flux examined in this study to prevent the occurrence of excessively high source temperatures. The high uniformity of thermal resistance across the cold plate indicates an almost independent heat removal from individual heaters with less interaction with other heaters. The porous nature of wick structures within the cold plate contributes to an increase in the number of menisci, thereby facilitating evaporation. This results in a decrease in thermal resistance. Moreover, the phase separator plays a crucial role in preventing flooded evaporators and then further lowering thermal resistance. Also, the capillary pressure generated by the wicks enhances the evaporator's rewetting capability, resulting in an increased upper limit for operation (i.e., CHF).

Pumping power is a critical parameter in the design of an active thermal management solution, as an increase in pumping power may hinder the use of the cooling system, irrespective of its capability to improve thermal performance [17]. The determination of pumping power involves multiplying the pressure drop across the system by the volume flow rate. Using appropriately sized transport tubes, efforts were made to minimize the pressure drop across the loop, concentrating the primary pressure drop within the cold plate. This pressure drop was calculated by taking the difference between the outlet pressure and the inlet pressure, measured by their respective pressure transducers. One of the significant merits of a HTPCS is that it requires a low flow rate to feed the evaporators for evaporation only, potentially reducing the pumping power. The HTPCS developed in this work operated within a low pumping power range, staying below 0.14 W.

Besides demonstrating significant hydrothermal performance, employing one single AM process for fabricating the entire cold plate substantially reduces production complexity and time compared to conventional manufacturing methods for fabricating similar cold plates. The combination of these merits positions the additively manufactured cold plate in this study as an appealing thermal management solution for future high-heat-flux electronics.

4. CONCLUSION

The thermal performance of a HTPCS, featuring seven heaters positioned randomly on the cold plate surface, was evaluated. The significance of the cold plate lay in (i) preventing flooded evaporators using phase separators, and (ii) fabricating the entire cold plate through one single AM process. The HTPCS operated at heat fluxes above 505 W/cm^2 and achieved thermal resistances ~ 0.16 K-cm^2/W. Furthermore, the cold plate operated with low pumping power below 0.14 W. Fabricating the entire cold plate through one single AM process enhances its overall technological appeal, making it well-suited for the commercialization of the HTPCS for the thermal management of high-heat-flux electronics.

ACKNOWLEDGEMENTS

Financial support by the Office of Science in the U.S. Department of Energy, award number DE-SC0018845 is gratefully acknowledged. The authors express their gratitude to Dr. Massoud Kaviany at the University of Michigan, Ann Arbor, for providing the SEM image of additively manufactured wicks.

REFERENCES

[1] Shaeri M R, Chen C-H, Bonner R W and Demydovych M 2023 Demonstration of CTE-Matched Two-Phase Minichannel Heat Sink *2023 22nd IEEE Intersociety Conference on Thermal and Thermomechanical Phenomena in Electronic Systems (ITherm)* (Orlando, FL, USA: IEEE) pp 1–5

[2] Fan S and Duan F 2020 A review of two-phase submerged boiling in thermal management of electronic cooling *Int. J. Heat Mass Transf.* **150** 119324

[3] Shaeri M R, Attinger D and Bonner R 2017 Feasibility study of a vapor chamber with a hydrophobic evaporator substrate in high heat flux applications *Int. Commun. Heat Mass Transf.* **86** 199–205

[4] Tang Y, Jia M, Ding X, Li Z, Wan Z, Lin Q and Fu T 2019 Experimental investigation on thermal management performance of an integrated heat sink with a piezoelectric micropump *Appl. Therm. Eng.* **161** 114053

[5] Adera S, Antao D, Raj R and Wang E N 2016 Design of micropillar wicks for thin-film evaporation *Int. J. Heat Mass Transf.* **101** 280–94

[6] Mudawar I 2013 Recent Advances in High-Flux, Two-Phase Thermal Management *J. Therm. Sci. Eng. Appl.* **5** 021012

[7] Dai X, Yang F, Yang R, Lee Y-C and Li C 2013 Micromembrane-enhanced capillary evaporation *Int. J. Heat Mass Transf.* **64** 1101–8

[8] Li W and Joshi Y 2020 Capillary-Assisted Evaporation/Boiling in PDMS Microchannel Integrated with Wicking Microstructures *Langmuir* **36** 12143–9

[9] Lee M and Park C 2022 Mechanical-capillary-driven two-phase loop: Feedback control for thin-film evaporation and capillary limit enhancement *Appl. Therm. Eng.* **204** 117960

[10] Yang F, Dai X, Kuo C-J, Peles Y, Khan J and Li C 2013 Enhanced flow boiling in microchannels by self-sustained

high frequency two-phase oscillations *Int. J. Heat Mass Transf.* **58** 402–12

[11] Lee J, Darges S J and Mudawar I 2021 Experimental investigation and analysis of parametric trends of instability in two-phase micro-channel heat sinks *Int. J. Heat Mass Transf.* **170** 120980

[12] Shaeri M R, Bonner R W and Ellis M C 2020 Thin hybrid capillary two-phase cooling system *Int. Commun. Heat Mass Transf.* **112** 104490

[13] Catuche J, Shaeri M R and Ellis M C 2022 Additive Manufacturing of Capillary-Driven Two-Phase Cold Plates *Proceedings of the 8th World Congress on Mechanical, Chemical, and Material Engineering (MCM'22)* (Czech Republic, Prague) p HTFF 174

[14] Shaeri M R, Bonner R and Catuche J 2023 Additively Manufactured Hybrid Two-Phase Cold Plate *ASME 2023 International Technical Conference and Exhibition on Packaging and Integration of Electronic and Photonic Microsystems* ASME 2023 International Technical Conference and Exhibition on Packaging and Integration of Electronic and Photonic Microsystems (San Diego, California, USA: American Society of Mechanical Engineers) p V001T07A001

[15] Bejarano R V and Park C 2014 Active flow control for cold-start performance enhancement of a pump-assisted, capillary-driven, two-phase cooling loop *Int. J. Heat Mass Transf.* **78** 408–15

[16] Geng Z and Bidanda B 2021 Geometric precision analysis for Additive Manufacturing processes: A comparative study *Precis. Eng.* **69** 68–76

[17] Shaeri M R, Sarabi S, Randriambololona A M and Shadlo A 2022 Machine learning-based optimization of air-cooled heat sinks *Therm. Sci. Eng. Prog.* **34** 101398